A novel approach for ramp-rate control of solar PV using energy storage to mitigate output fluctuations caused by cloud passing

M J. E Alam
University of Wollongong, mjealam@uowmail.edu.au

K M. Muttaqi
University of Wollongong, kashem@uow.edu.au

D Sutanto
University of Wollongong, soetanto@uow.edu.au

A novel approach for ramp-rate control of solar PV using energy storage to mitigate output fluctuations caused by cloud passing

Abstract

The variability of solar irradiance with a high ramp-rate, caused by cloud passing, can create fluctuation in the PV output. In a weak distribution grid with a high PV penetration, this can create significant voltage fluctuations. Energy storage devices are used to smooth out the fluctuation using traditional moving average control. However, moving average does not control the ramp-rate directly; rather the ramp-rate depends on previous values of PV output. This paper proposes a strategy where the ramp-rate of PV panel output is used to control the PV inverter ramp-rate to a desired level by deploying energy storage (which can be available for other purposes, such as storing surplus power, countering voltage rise, etc.). During the ramping event, the desired ramp-rate is governed by controlling the energy storage based on an inverse relationship with the PV panel output ramp-rate to improve the fluctuation mitigation performance. In contrast to the moving average method, the proposed strategy is able to control the desired ramp-rate independent of the past history of the PV panel output. A dynamic model of the PV-storage integrated system is developed to verify the proposed strategy in the presence of physical device time lags. The proposed strategy is verified using simulation results based on an Australian distribution system. A laboratory experiment is also conducted to validate the concept of the proposed control strategy.

Keywords

Disciplines

Engineering | Science and Technology Studies

Publication Details

A Novel Approach for Ramp-rate Control of Solar PV Using Energy Storage to Mitigate Output Fluctuations Caused by Cloud Passing

M. J. E. Alam, *Student Member, IEEE*, K. M. Muttaqi, *Senior Member, IEEE* and D. Sutanto, *Senior Member, IEEE*

Abstract— The variability of solar irradiance with a high ramp-rate, caused by cloud passing, can create fluctuation in the PV output. In a weak distribution grid with a high PV penetration, this can create significant voltage fluctuations. Energy storage devices are used to smooth out the fluctuation using traditional moving average control. However, moving average does not control the ramp-rate directly; rather the ramp-rate depends on previous values of PV output. This paper proposes a strategy where the ramp-rate of PV panel output is used to control the PV inverter ramp-rate to a desired level by deploying energy storage (which can be available for other purposes, such as storing surplus power, countering voltage rise, etc). During the ramping event, the desired ramp-rate is governed by controlling the energy storage based on an inverse relationship with the PV panel output ramp-rate to improve the fluctuation mitigation performance. In contrast to the moving average method, the proposed strategy is able to control the desired ramp-rate independent of the past history of the PV panel output. A dynamic model of the PV-storage integrated system is developed to verify the proposed strategy in the presence of physical device time lags. The proposed strategy is verified using simulation results based on an Australian distribution system. A laboratory experiment is also conducted to validate the concept of the proposed control strategy.

Index Terms— Solar PV, fluctuation, ramp-rate control, energy storage.

I. INTRODUCTION

SOLAR photovoltaic power generation can be highly variable in nature due to the irregularities in the sun irradiance level caused by cloud passing. Although the investigation on PV output variability has been continuing for a long time as evidenced in [1-2], it is still being addressed as an issue of contemporary interest [3], especially with a high penetration level of PV resources. Recent operating experiences from La Ola Island PV plant [4] has revealed that the ramp-rate of the PV output can be as high as 63% of the rated capacity/minute, whereas it was intended to limit the ramp-rate up to 30% of the rated capacity /minute [4]. To avoid any negative impact of such a high ramp-rate on the

distribution system, the PV penetration was limited to 50% of the PV plant capacity [4]. The one-second resolution irradiance data collected from Oahu Island by NREL [5] shows that the irradiance level can fluctuate with a ramp-rate of more than 50% between two consecutive measurements. A PV output ramp-rate of 20% of the rated capacity/second is recorded in a study [6] conducted on a system in Mesa del Sol, New Mexico. In Australia, the Commonwealth Scientific and Industrial Research Organisation (CSIRO) has reported [7] that the PV output ramp-rates can be up to 8% of the rated capacity/second at various locations. With a high penetration of grid-connected PV resources in weak radial distribution systems, such high ramp-rate variations of the PV output can introduce significant voltage fluctuations [8]. Therefore, ramp-rate control strategies to reduce fluctuations in PV outputs and the resulting voltage fluctuations in PV integrated distribution systems are necessary in order to increase the PV penetration level in the networks.

Different kinds of energy storage technologies have been proposed for smoothing of PV output, such as, electric double-layer capacitor (EDLC) [9-11], superconducting magnetic energy storage [12], fuel cell [13], and battery energy storage [14-15]. A moving average based ramp-rate control is proposed in [9] for smoothing PV output fluctuations using EDLC. The moving average method was also used in [14] for controlling battery energy storage to reduce PV fluctuations. An exponential moving average has been used in [16] that gives more weight on the recent values of the fluctuating PV output. A modified Euler type moving average model is proposed in [11] for prediction of moving average values for a hybrid system with PV, fuel cell, EDLC and battery. Controlling an energy storage device using traditional moving average method can reduce PV output fluctuation, but it may not necessarily control the PV output to a desired ramp-rate. Also, a moving average with a long averaging window would require a storage device to operate to match the difference between the actual PV output and the moving average, even if the actual PV output is not significantly fluctuating. The battery and charging facility available in an electric-vehicle has been used in [15] to mitigate the short-term intermittency using a high-pass filter for fluctuation mitigation. In this method, the ramp-rate of PV inverter is limited using the characteristics of the filter, such as the corner frequency. A dynamic filtering controller and dynamic rate limiter approach

is used in [17] for smoothing of PV and wind power generation fluctuations.

In [18], the power delivered/absorbed by energy storage for ramp-rate control is determined using a battery State of Charge (SoC) versus allowable ramp-rate droop characteristic for generic renewable resources, where the allowable ramp-rate is related to the SoC, but not directly related to the renewable resource ramp-rate. An application of this strategy for a utility scale PV plant is demonstrated in [19]. Fluctuation mitigation using moving average control and a first-order low pass filter is presented in [20] where the SoC of the energy storage device is maintained within a range by modifying the energy storage power output using a gain parameter, which requires tuning. The impact of different storage time constants has also been investigated using time constants up to 30 seconds. Authors in [6] have applied both ramp-rate control and moving average method for intermittency mitigation of the aggregate output of a distribution system with several distributed resources including an energy storage system. There is no unique strategy for PV output smoothing, as it depends on many factors including cost and response time of the compensating resource and system operation policy [6]. Also, the delay in data transmission can cause less smooth output or may even add more fluctuation to the aggregate output [6]. However, if the fluctuation is mitigated at the PV connection point with local information, the transmission of data would not be necessary.

The contribution of this paper is to propose a new method for mitigation of PV inverter output fluctuation by ramp-rate control using energy storage. The energy storage system may be available for other purposes, such as storing excess energy for use when the sun is not available, mitigating voltage rise, etc [21]. The novelty of the proposed approach is an algorithm to control the ramp-rate of the PV output fluctuation using the appropriate strategies during the ramping and post-ramping event. During a ramp-down or ramp-up event, the energy storage system is controlled based on an inverse characteristic of the desired ramp-rate of PV inverter with respect to the ramp-rate of the PV panel output to improve the fluctuation mitigation performance. Once the ramping event is over, the energy storage system will be controlled using a SoC droop characteristic to consider the available capacity in selecting the desired ramp-rate. Unlike the traditional moving average method, the proposed strategy does not have a memory effect and therefore the storage devices can be controlled according to the requirement at each instant of time without being influenced by the PV panel output at the previous instants or without affecting the compensating power at a future time instant. A dynamic model of the PV-storage integrated system is developed and integrated with the distribution network model to test the validity of the proposed strategy in a dynamic environment with physical device time-lags. Voltage fluctuation mitigation achieved by applying the proposed control strategy is also investigated. The proposed control strategy is verified using a daylong quasi-steady-state and dynamic simulation based on an Australian distribution system and also using a basic experimental setup.

II. LIMITATIONS OF TRADITIONAL MOVING AVERAGE METHOD IN RAMP-RATE CONTROL

Traditionally, moving average is used to smooth out a fluctuating variable. Energy storage device has been controlled by moving average method for smoothing PV output fluctuations in [14, 20]. Although this is a traditionally accepted way to reduce the fluctuations in PV output, it requires the energy storage device to inject/absorb power even if the PV output is not fluctuating significantly. Also, such moving average strategy does not control the ramp-rate directly. These points are discussed further below.

It is well-known that moving average has a memory effect. Depending on the length of the averaging window, a moving average would highly depend on the past history and therefore, may be significantly different than the present value of the fluctuating variable. For PV output smoothing, the integrated storage device will have to operate to make-up for the aforementioned difference between the actual PV output and the moving average. Numerically, a moving average with a w-length window contains only $(1/w)$ % of the present value of the fluctuating variable. A realistic PV output from Oahu Island, Hawaii on the 18th of March 2010, available from NREL [5] and its 20-min moving average is shown in Fig. 1. Although the PV output does not fluctuate significantly during the time periods in the red circles, the moving average values during these times still deviate significantly from the actual PV outputs due to the memory effect of the moving average method. To make-up for this deviation, energy storage device needs to operate more than necessary.
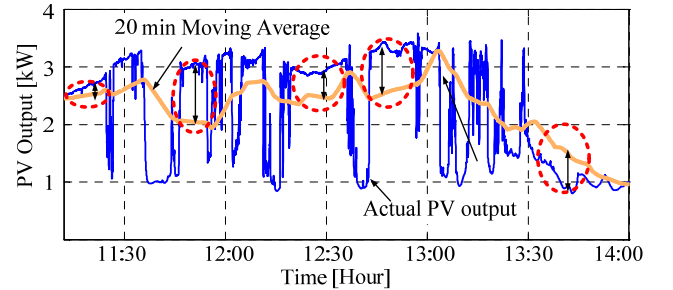

Fig. 1. Actual PV output and a 20-min moving average.

Further, with a given window length w, the moving average method may not provide a desired ramp-rate; rather the ramp-rate will depend on the past history of the fluctuating PV output. The ramp-rate of the moving average of a variable PV output at the k-th time instant can be defined using the following expression.

$$MoRR(k) = \frac{1}{w} \times \frac{\sum_{i=0}^{w-1} P_{DC}(k-i) - \sum_{i=0}^{w-1} P_{DC}(k-1-i)}{t(k) - t(k-1)}$$

$$= \frac{1}{w} \times \frac{P_{DC}(k) - P_{DC}(k-w)}{t(k) - t(k-1)} \quad (1)$$

where, $MoRR(k)$ is the ramp-rate of the moving average of PV panel DC output, w is the length of the moving average window in terms of the number of data points, P_{DC} is the PV panel DC output and $t(k)$ is the time corresponding to the k-th time instant. Observing (1), it is clear that the ramp-rate obtained by following a moving average of the PV output

depends on the PV output at the k-th and $(k\text{-}w)$-th instant. Although, a significantly low ramp-rate can be obtained by following a moving average with a long window, it is not directly related to the actual desired level.

III. THE PROPOSED RAMP-RATE CONTROL STRATEGY

A. Concept of the Proposed Ramp-rate Control Strategy

In the proposed ramp-rate control strategy, a compensation power will be added with the PV panel DC power to control the ramp-rate of the PV inverter output within a desired level at any instant of time. The basic concept of ramp-rate control strategy is explained in Fig. 2.
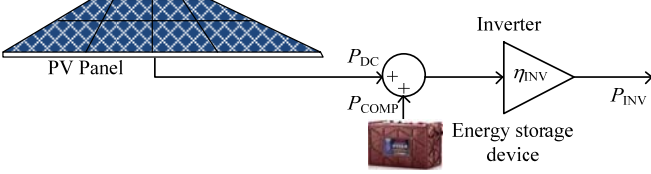

Fig. 2. Conceptual schematic of the proposed ramp-rate control strategy.

Based on Fig. 2, the PV inverter output P_{INV} can be obtained from the PV panel DC power P_{DC} and the compensation power P_{COMP} using the following expression.

$$P_{INV} = \eta_{INV} \times (P_{DC} + P_{COMP}) \tag{2}$$

In Fig. 2 and (2), η_{INV} is the inverter efficiency. Taking time derivative of (2) at both sides, the ramp-rate of P_{INV} can now be related with the ramp-rate of P_{COMP} and P_{DC}, as given in (3).

$$\frac{dP_{INV}}{dt} = \eta_{INV} \times \left[\frac{dP_{DC}}{dt} + \frac{dP_{COMP}}{dt} \right] \tag{3}$$

where, $\dfrac{dP_{INV}}{dt}$ is the PV inverter output ramp-rate, $\dfrac{dP_{DC}}{dt}$ is

the PV panel DC power output ramp-rate, and $\dfrac{dP_{COMP}}{dt}$ is the

compensation power ramp-rate.

To control the ramp-rate of the PV inverter output within a desired level, the ramp-rate of P_{COMP} can be controlled using the expression derived from (3), as given below.

$$\frac{dP_{COMP}}{dt} = \frac{1}{\eta_{INV}} \times \left[\left. \frac{dP_{INV}}{dt} \right|_{des} - \eta_{INV} \times \frac{dP_{DC}}{dt} \right] \tag{4}$$

where, $\left. \dfrac{dP_{INV}}{dt} \right|_{des}$ is the desired ramp-rate of the PV inverter,

which will be negative during a ramp-down event and positive during a ramp-up event.

The expression given in (4) is the basic control equation that will be followed to control the ramp-rate of PV inverter output. However, the following modifications are made to accommodate practical situations.

(a) To allow for the slow variations of P_{DC} with the progress of the day, a dead-band function 'f' is incorporated with (4) that will force the ramp-rate of P_{DC} to be *zero* if it is within an acceptable limit, defined using the desired ramp-rate of P_{INV}, as shown below.

$$f\left(\frac{dP_{DC}}{dt} \right) = \begin{cases} 0, \text{if } \eta_{INV} \times \left| \dfrac{dP_{DC}}{dt} \right| \leq \left. \dfrac{dP_{INV}}{dt} \right|_{des} \\[3mm] \dfrac{dP_{DC}}{dt}, \text{otherwise} \end{cases} \tag{5}$$

(b) Observing (4) it is apparent that when the ramp-rate of P_{DC} is *zero*, considering the dead-band function mentioned in modification (a), the ramp-rate of P_{COMP} will be governed by the desired ramp-rate of P_{INV}. However, when the ramp-rate of P_{DC} is *zero*, then if P_{COMP} has already attained such a level that removal of P_{COMP} would not create an unacceptable fluctuation in P_{INV}, then P_{COMP} does not need to be changed anymore. To accommodate this, a switching function S, as given below, is incorporated with (4).

$$S = \begin{cases} 0, \text{if } |P_{COMP}| < \left. \dfrac{dP_{INV}}{dt} \right|_{des} \text{ and } f\left(\dfrac{dP_{DC}}{dt} \right) = 0 \\[3mm] 1, \text{otherwise} \end{cases} \tag{6}$$

The modified control equation can be described using the expression below.

$$\frac{dP_{COMP}}{dt} = S \times \left[\frac{1}{\eta_{INV}} \times \left\{ \left. \frac{dP_{INV}}{dt} \right|_{des} - \eta_{INV} \times f\left(\frac{dP_{DC}}{dt} \right) \right\} \right] \tag{7}$$

The inverter efficiency η_{INV} will depend on the power output of the inverter. The efficiency curve for a given inverter over a range of operating power can be obtained from the manufacturer or developed through testing. As the desired P_{INV} at any given instant is known, η_{INV} at the desired P_{INV} can be taken from the efficiency curve and can be used in (7) to control the ramp-rate of P_{COMP} at the necessary level.

Considering a discrete time representation, the ramp-rate of P_{DC} at the k-th instant can be determined using the expression below.

$$\frac{dP_{DC}}{dt}(k) = \frac{[P_{DC}(k) - P_{DC}(k-1)]}{t(k) - t(k-1)} \tag{8}$$

where, $t(k)$ is the time at the k-th instant.

The value of the switching function is also incorporated with P_{COMP} to force it to *zero* when the conditions of $S = 0$ are satisfied, as given in (6). P_{COMP} at the k-th instant can be obtained using (9).

$$P_{COMP}(k) = S \times \left[P_{COMP}(k-1) + \frac{dP_{COMP}}{dt}(k) \times \{ t(k) - t(k-1) \} \right] \tag{9}$$

To illustrate the proposed ramp-rate control strategy, a fictitious PV output fluctuation shown in Fig. 3(a) is used, where the PV panel output decreases at a ramp-rate of PVRR$_1$ kW/sec from time t_1 to t_2, remains constant at the level reached at time t_2 up to time t_3, and again increases from time t_3 to time t_4 at a ramp-rate of PVRR$_2$ kW/sec. After reaching time t_4, the PV output remains constant. To control the ramp-rate of P_{INV}, (7) and (9) are used to produce the appropriate amount of P_{COMP}. The desired ramp-rate of P_{INV} is defined as the Maximum Allowable Ramp-rate (MARR) in W/sec. To apply the proposed strategy to any size of PV plant, the ramp-rate units can also be defined in % of the rated PV capacity/sec. Before time t_1, P_{DC} remains at a stable state. Therefore, the ramp-rate of P_{COMP} is *zero* according to (7), and remains *zero*. From time t_1 to t_2, P_{DC} sharply decreases with a ramp-rate of

PVRR$_1$. During this time the ramp-rate of P_{COMP} is determined using PVRR$_1$ and MARR. At time t_2, PVRR$_1$ becomes *zero*, but P_{COMP} is not *zero* yet. Therefore, the ramp-rate of P_{COMP} from time t_2 to t_3 is determined using MARR only. From time t_3 to t_4, P_{DC} sharply increases with a ramp-rate of PVRR$_2$. During this time, P_{COMP} is controlled with a ramp-rate determined using PVRR$_2$ and MARR. After time t_4, PVRR$_2$ becomes *zero*, however, P_{COMP} is not *zero* yet. Therefore, from time t_4 P_{COMP} is controlled using MARR only. At time t_5, P_{COMP} becomes *zero* and the ramp-rate of P_{DC} is also *zero*. Therefore, the ramp-rate of P_{COMP} is *zero* after t_5 which keeps P_{COMP} at *zero*.
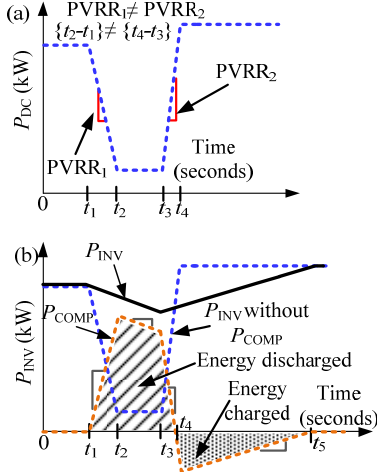

Fig. 3. An illustration of the proposed ramp-rate control strategy. (a) A hypothetical PV output fluctuation. (b) PV inverter output with appropriately controlled P_{COMP} to limit the P_{INV} ramp-rate within a desired level.

For moving average control, P_{COMP} at a given k-th instant depends on the previous values of P_{DC} within the averaging window, w, as given below.

$$P_{COMP}(k) = \frac{\sum_{i=0}^{w-1} P_{DC}(k-i)}{w} - P_{DC}(k) \qquad (10)$$

Therefore, if moving average is applied to control the ramp-rate of the fluctuation shown in Fig. 3(a), then P_{COMP} at $t > t_1$ will actually depend on the P_{DC} values before t_1. It will not directly depend on the required P_{COMP} to control the ramp-rate at a desired level. According to (10), P_{COMP} is only controllable using the length of the averaging window w. The higher the number w is chosen, the more is the smoothing effect. However, if a high w is chosen for improving fluctuation mitigation performance at the k-th instant, it not only impacts the P_{COMP} at the k-th instant, but also at all the future time instants. For example, if w is increased by Δw to increase the smoothing effect at the k-th instant, then at any future $(k+j)$-th instant, the deviation of P_{COMP} due to the increase of w (i.e., Δw) will be,

$$\Delta P_{COMP}(k+j) = \left| \frac{\sum_{i=0}^{w+\Delta w-1} P_{DC}(k+j-i)}{w+\Delta w} - \frac{\sum_{i=0}^{w-1} P_{DC}(k+j-i)}{w} \right| \qquad (11)$$

The deviation ΔP_{COMP} at the $(k+j)$-th instant is solely due to the increase of w at the k-th instant. For a given Δw, this

deviation will remain in effect for all future time instants even if it is not necessary because of acceptable variations in P_{DC}.

In contrast, according to the proposed ramp-rate control strategy, the amount of P_{COMP} to control the ramp-rate at a given k-th instant can be governed by the desired ramp-rate of P_{INV} for the k-th instant only and it does not impact the future ramp-rates. According to (9), P_{COMP} at the k-th time instant is,

$$P_{COMP}(k) = S \times \left[P_{COMP}(k-1) + \phi\left(\left. \frac{dP_{INV}}{dt}(k) \right|_{des} \right) \right] \qquad (12)$$

In (12), $\phi(\cdot)$ denotes a function that determines the ramp-rate of P_{COMP} for obtaining the desired ramp-rate of P_{INV} at the given ramp-rate of P_{DC}. The value of $\phi(\cdot)$ is obtained using (7). As the proposed strategy does not have a memory effect, P_{COMP} can be changed at each instant dynamically based on the requirement. This advantage is used in this paper to improve the fluctuation mitigation performance.

B. Improvement of the Fluctuation Mitigation Performance

For a given PV output fluctuation, the duration of the ramping event is inversely proportional to the ramp-rate of the PV output, because the higher the ramp-rate, the faster the PV output changes from one stable state to another stable state. As the time duration for a high-rate ramping event is very short, the amount of energy needs to be used for ramp-rate control is small. Therefore, during the ramping event, the MARR can be reduced in an inverse proportion to the PV panel output ramp-rate (PVRR) to improve the fluctuation mitigation performance without discharging a significant amount of storage capacity. Such an inverse characteristic is given in (13) and shown in Fig. 4(a).

$$\text{MARR}_\rho(k) = \begin{cases} |\text{PVRR}(k)|, \text{ if } |\text{PVRR}(k)| < \text{RR}_{lim} \\ \dfrac{\gamma}{|\text{PVRR}(k)|}, \text{ if } |\text{PVRR}(k)| \geq \text{RR}_{lim} \end{cases} \qquad (13)$$

In (13), MARR_ρ is the inverse characteristic based desired ramp-rate, to be applied during the ramping event and γ is a factor to control the degree of inverse characteristic; RR_{lim} is a threshold of ramp-rate of P_{DC} beyond which the inverse characteristic is applied. RR_{lim} should be set to a value higher than the ramp-rate of slow variations of P_{DC} to allow P_{INV} to vary with the progress of the day. Once the ramping event is over, the P_{COMP} can be brought to *zero* with an MARR determined using a SoC droop characteristic as given by (14) and shown in Fig. 4(b).

$$\text{MARR}_\sigma(k) = \begin{cases} \text{MARR}_{min}, \text{ if } |\Delta\text{SoC}(k)| < \text{SoC}_{LB} \\ \text{MARR}_{min} + \dfrac{DB_{MARR}}{DB_{SoC}} \times \left[|\Delta\text{SoC}(k)| - \text{SoC}_{LB} \right], \\ \qquad \text{if } \text{SoC}_{LB} \leq |\Delta\text{SoC}(k)| \leq \text{SoC}_{UB} \\ \text{MARR}_{max}, \text{ if } |\Delta\text{SoC}(k)| > \text{SoC}_{UB} \end{cases} \qquad (14)$$

In (14), MARR_σ is a SoC droop based desired ramp-rate, to be applied once the ramping event is over; DB_{MARR} and DB_{SoC} are the dead-bands of MARR and SoC, respectively; SoC_{LB} and SoC_{UB} are the lower and upper bands of SoC, respectively, and $|\Delta\text{SoC}(k)|$ is the absolute value of the deviation between $\text{SoC}(k-1)$ and a user defined reference SoC_{ref}. Using the absolute deviation makes the droop

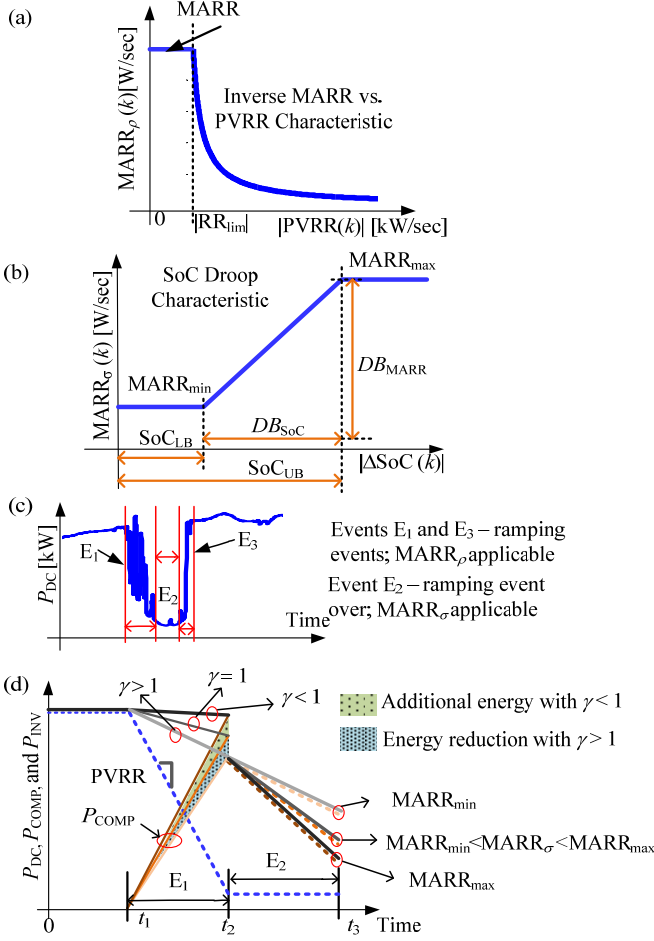characteristic applicable for change of SoC in either direction.

Fig. 4. Ramping event dependent selection of MARR. (a) During the ramping event. (b) After the ramping event. (c) Application of $MARR_\rho$ and $MARR_\sigma$ (d) The effect of γ and MARR versus SoC droop on ramp-rate control.

Fig. 4(c) identifies the ramping events in a real PV output fluctuation and shows the event driven application of $MARR_\rho$ and $MARR_\sigma$ to control the ramp-rates. SoC_{LB} defines the amount of energy available for controlling the ramp-rate at $MARR_{min}$ before entering the droop characteristic. Therefore, SoC_{LB} should be set to a value that represents a sufficient amount of energy to control the ramp-rate at $MARR_{min}$ (during the worst-case fluctuation) for a certain amount of time that allows for any back up power to come online or any sensitive load to be shut down safely. SoC_{UB} should be set up to a value that represents a substantial portion of the energy needed to control the ramp-rate (during the worst-case fluctuation) before exceeding the saturation limit of the droop characteristic ($MARR_{max}$).

The effect of the parameter γ in (13) and the parameters $MARR_{min}$ and $MARR_{max}$ in (14) on the fluctuation mitigation performance is shown in Fig. 4(d) using a fictitious PV fluctuation containing a ramping event E_1 (time t_1 to t_2) at a ramp-rate PVRR, followed by a low PV event E_2 (time t_2 to t_3). During the event E_1, $MARR_\rho$ is applicable which is determined by γ. If $\gamma = 1$, $MARR_\rho$ is in direct inverse relation with the ramp-rate of P_{DC}. If $\gamma < 1$, the degree of the inverse characteristic increases, and therefore, P_{INV} is improved

compared to $\gamma = 1$. However, this will be performed at the expense of additional energy discharged from the storage device as shown in Fig. 4(d) using the shaded region. If $\gamma > 1$, the degree of the inverse characteristic decreases, and therefore, P_{INV} is reduced compared to $\gamma = 1$, but at the same time less amount of energy is discharged from the storage device, as shown in Fig. 4(d). Although for high ramp-rate events, the variation of storage energy discharge is not significant, it provides the user a control over the fluctuation mitigation performance of the proposed strategy.

During the event E_2, P_{COMP} slowly decreases at $MARR_\sigma$ determined from the SoC droop characteristic in (14). For a given fluctuation, $MARR_{min}$ is selected as $MARR_\rho$ so that P_{INV} can be reduced at the same ramp-rate as it reduces during event E_1, which provides a smooth transition in ramp-rate control from event E_1 to E_2. However, if $|\Delta SoC|$ is higher than SoC_{LB}, then $MARR_\sigma$ is increased and therefore, P_{INV} reduces at a higher ramp-rate as shown in Fig. 4(d). $MARR_{max}$ in (14) needs to be set to a value that allows for the slow variations of P_{DC}, as mentioned for selecting RR_{lim} in (13).

The discussions presented above provide only basic guidelines for selection of the control parameters for the proposed strategy. In general, these parameters are user defined and can vary depending on the scenario.

C. Energy Utilization for the Control of Ramp-rate

The amount of energy to be utilized by an energy storage device for controlling the ramp-rate will mainly depend on the PV panel output power, P_{DC}, just prior to start of the fluctuation, and the maximum allowable ramp-rate, MARR. A relation of the energy usage for ramp-rate control to the rated output of a PV panel is established and discussed below using Fig. 5.
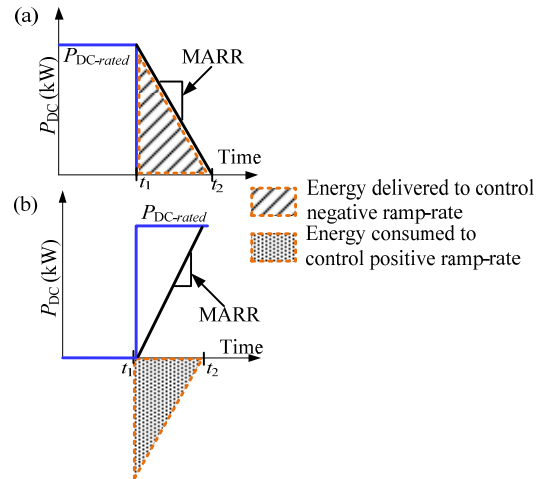

Fig. 5. Energy utilization in the proposed ramp-rate control strategy. (a) During negative ramp-rate control; (b) During positive ramp-rate control.

To consider a worst case fluctuation, a PV output power having a sudden fall from the rated value of $P_{DC\text{-}rated}$ to *zero* at time t_1 is shown in Fig. 5(a). In this case it is assumed that P_{DC} does not return to its previous value due to a likely phenomenon of a sustained cloudy period, after time t_1. According to the proposed strategy, the PV inverter output will be slowly reduced at the maximum allowable ramp-rate

MARR and will become *zero* at time t_2, instead of suddenly dropping to *zero*. The value of MARR will be determined depending on the situation as shown in Fig. 4. The energy to be discharged by the storage device in controlling the ramp-rate is shown in Fig. 5(a) using a shaded area. A similar type of worst case scenario for positive ramp-rate is shown in Fig. 5(b), where the PV output suddenly increases from *zero* to $P_{DC\text{-}rated}$ at time t_1. In this case, the positive ramp-rate of the P_{INV} is controlled by charging the energy storage with certain amount of energy, as indicated using a shaped area in Fig. 5(b). The energy utilized for ramp-rate control, E_{RRC} (kWh) can be derived using the expression given below.

$$E_{RRC} = \frac{\sum_{i=1}^{N_{tot}}(P_{DC\text{-}rated} - i \times \text{MARR})}{3600} \qquad (15a)$$

where, N_{tot} is the total number of time-steps between time t_1 (seconds) and t_2 (seconds), which can be determined using,

$$N_{tot} = \frac{P_{DC-rated}}{\text{MARR}} \qquad (15b)$$

In (15a), 3600 is used to bring the unit to kWh, as the calculations are being performed in per second unit. A plot of the E_{RRC} for rated PV capacities up to 5 kW is derived using (15) for different values of MARR and is shown in Fig. 6. Increase of energy utilization for ramp-rate control with increase in PV capacity and decrease in MARR is observed in Fig. 6.
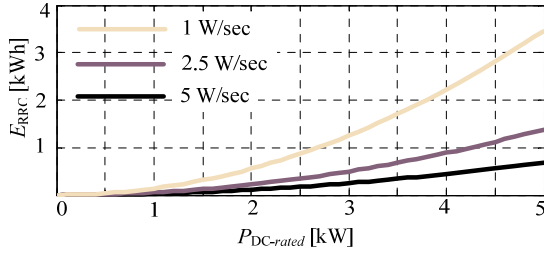

Fig. 6. Variations of the energy utilization for ramp-rate control with different rated PV output at different MARR.

Instead of using $P_{DC\text{-}rated}$, $P_{DC}(k)$ can be used in (15) to determine the energy required to control the ramp-rate from the present value of P_{DC}. The amount of energy determined in this way can be identified as an Energy Buffer (E_{Buff}) to approximately check the minimum amount of capacity need to be present in the storage to control the ramp-rate according to the proposed strategy.

D. The Flow Chart of the Proposed Control Strategy

The flowchart of the proposed ramp-rate control strategy for a given k-th time instant is shown in Fig. 7. The ramp-rate of P_{DC} at the k-th instant PVRR(k) is calculated using (8), and based on this MARR$_\rho$ is calculated using (13). If PVRR(k) is equal to or higher than MARR$_\rho$, S is set to 1 and the ramp-rate of P_{COMP} is determined using (7) and in this case the desired ramp-rate is replaced with MARR$_\rho$. If PVRR(k) is found lower than MARR$_\rho$, then a test is performed to find if removal of P_{COMP} would create an unacceptable fluctuation in P_{INV}. If 'Yes', then S is set to 1 and the ramp-rate of P_{COMP} is determined using (7), but in this case the desired ramp-rate is replaced with MARR$_\sigma$, determined from (14). If 'No', then the

ramp-rate of P_{COMP} is determined using (7) with $S = 0$. The ramp-rate of $P_{COMP}(k)$ is applied to determine $P_{COMP}(k)$ using (9). With the value of $P_{COMP}(k)$ obtained, the present level of SoC is checked. If it is found within the lower (SoC$_{LL}$) and upper (SoC$_{UL}$) limits of SoC, obtained using the Maximum Depth of Discharge (DoD$_{max}$), the Maximum State of Charge (SoC$_{max}$), and buffer energy E_{Buff}, then a charge/discharge operation is performed depending on the sign of $P_{COMP}(k)$. According to the proposed strategy, a +*ve* sign means discharge, and –*ve* sign means charge. Once the discharging/charging decision for the time instant is made and the storage is put into operation, the control system proceeds with a transition into the next time instant.
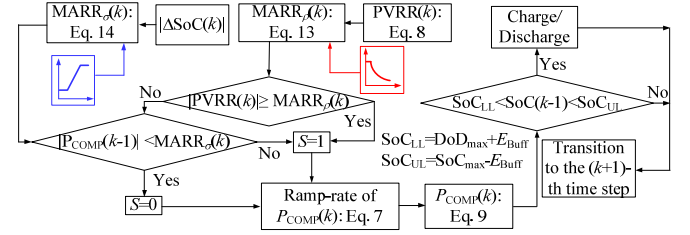

Fig. 7. Flow chart of the proposed ramp-rate control strategy.

Although this paper has mainly concentrated on the application of battery energy storage, the fundamental idea of ramp-rate control proposed in this paper would be applicable for other type of energy storage (such as ultra-capacitor).

E. Dynamic Model of PV-Storage Integrated System

The development of a dynamic model is necessary to understand the performance of the proposed strategy in the context of practical system components that are subject to physical device time lags. Detailed switching models of the power electronic converters are used in power-electronics based investigations where sub-cycle phenomena are of interest. However, for the scope of the investigations of this paper, such fast dynamics are not of interest. Therefore, a simplistic dynamic model of the PV-storage integrated system is developed, as shown in Fig. 8, that represents the time-lag related to the associated devices and components.
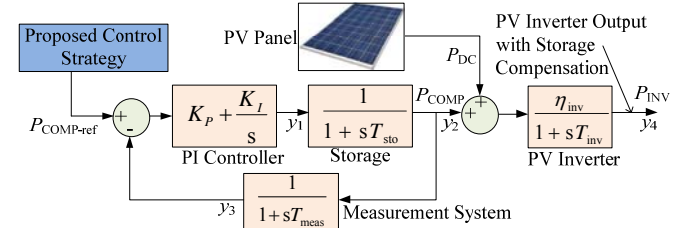

Fig. 8. A dynamic model of the PV-storage integrated system to consider the effect of physical device time-lags.

The dynamic model consists of four states which are the PI controller output (y_1), the storage power output (y_2), storage power output measurement signal (y_3), and the PV inverter output (y_4). The state equations are given below.

$$\frac{dy_1}{dt} = -K_P \times \frac{1}{T_{meas}} \times (y_2 - y_3) + K_I \times (P_{COMP\text{-}ref} - y_3) \qquad (16a)$$

$$\frac{dy_2}{dt} = \frac{1}{T_{sto}} \times (y_1 - y_2) \qquad (16b)$$

$$\frac{dy_3}{dt} = \frac{1}{T_{meas}} \times (y_2 - y_3) \qquad (16c)$$

$$\frac{dy_4}{dt} = \frac{1}{T_{inv}} \times (\eta_{inv}[P_{DC} + y_2] - y_4) \qquad (16d)$$

where, $P_{COMP\text{-}ref}$ is the reference to the PI controller; T_{inv} is the inverter time constant; T_{sto} is the storage time constant; T_{meas} is the storage output measurement circuit time delay; K_P and K_I proportional and integral gain of the PI controller.

It is necessary that the energy storage device responds to the charging/discharging commands as fast as possible to control the ramp-rate satisfactorily. Studies have shown that battery energy storage devices, such as NaS, Li-ion, and Valve-Regulated Lead-Acid (VLRA) batteries, have response time in the order of milliseconds [22-23]. Therefore, it is expected that with an appropriate selection of the energy storage device, the ramp-rate can be controlled according to the requirements. Using the developed dynamic model, the impact of different storage response times on ramp-rate control can be investigated.

The PI controller is tuned to have a low rise time so that the fast response time of the storage device can be effectively used for fluctuation mitigation. The initial controller parameters are obtained using the open-loop frequency response of the linearized plant model. The tuning task is performed with the aid of Simulink Automatic PID tuner [24] that performs the initial tuning based on a reference tracking algorithm while keeping a trade-off between performance and robustness. Once the initial parameters are obtained, further tuning is performed to reduce the rise time.

This paper has mainly discussed the concept of the proposed strategy and its system level application. To carry out a component level detailed design, practical issues, such as battery power losses, heat generated, and DC-link voltage fluctuations caused by high current pulses during high-ramp rate operations, need to be considered.

IV. APPLICATION EXAMPLE OF THE PROPOSED RAMP-RATE CONTROL STRATEGY

To analyze the performance of the proposed strategy in a distribution network environment, a low voltage (LV) distribution feeder extracted from the New South Wales distribution system is considered. All the households in the LV feeder are assumed to have rooftop PV units with integrated battery storage devices. A typical 12 kWh Valve Regulated Lead Acid battery is used for simulation. Energy storage devices are modeled incorporating the non-linear voltage versus SoC characteristics and the effect of internal resistance, as described in [21]. The LV feeder under study is shown in Fig. 9. The results shown correspond to the PV output fluctuations in household no. 28 (HH 28) connected to phase a, bus 10 of the LV feeder.

The PV output data correspond to the irradiance profile of the 18th of March, 2010, captured by NREL in the Oahu Island, Hawaii [4]. For simplicity, constant inverter efficiency (89.5%) is used in the simulations. To select the ramp-rate threshold limit to apply the inverse characteristic in (13), RR_{lim}

is selected by observing the ramp-rate during slow variation of P_{DC} from 7:00 hours to 9:00 hours. During this time frame, more than 99% of the ramp-rates were less than 3 W/sec, as

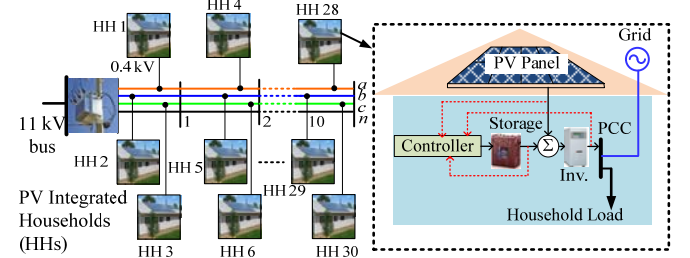Fig. 9. The LV test feeder with the PV-storage integrated systems.

shown in Fig. 10(a). Therefore, to allow for this variation, RR_{lim} is set to a higher value of 5 W/sec. $MARR_{max}$ in (14) is also set to 5 W/sec for the same purpose. Simulation trials have been run using a range of $0.1 \leq \gamma \leq 50$. For $\gamma \leq 1$, fluctuation mitigation performance does not improve much, whereas with $\gamma > 1$, deterioration of the fluctuation mitigation performance appears with $\gamma \geq 20$. The value of γ has been selected as 5 (with Watt to kW conversion: 0.005).
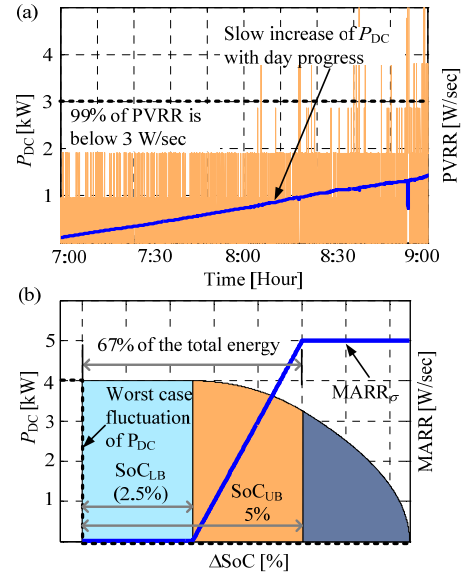

Fig. 10. PVRR during slow variation with the progress of the day. (a) Energy used to control the worst case fluctuation and $MARR_\sigma$ characteristic.

The storage devices are allowed to operate between a typical range of 40% to 100% SoC. To allow for charging and discharging for ramp-rate control, SoC_{ref} is set to 70%, which is at the mid-point of the allowable range of SoC. The SoC bands, SoC_{LB} and SoC_{UB}, are selected considering the worst case fluctuation of P_{DC} from the rated value (4 kW for the PV systems in the network under study) to $zero$ at the worst-case ramp-rate of $P_{DC\text{-}rated}$/sec and after the fall, P_{DC} does not recover due to a continuous cloudy period. The P_{DC} profile with the storage support is shown in Fig. 10(b), where the ramp-rate control is performed according to (14), as shown using the $MARR_\sigma$ profile. SoC_{LB} is set to 2.5% which corresponds to the amount of energy that can control the ramp-rate at the value of $MARR_{min}$ for about 5 minutes which is sufficient for bringing emergency power online or

disconnecting sensitive loads safely. SoC_{UB} is set to 5% which accounts for about 67% of the total energy used for bringing P_{DC} to zero at a controlled ramp-rate. The parameters used for the simulation of the proposed ramp-rate control strategy are given in Table-I in the Appendix. Initially, the results of the quasi-steady state simulations using 1-sec resolution data are presented to investigate the validity of the strategy over a daylong variation. Later, dynamic simulation results in milliseconds time-frame are presented.
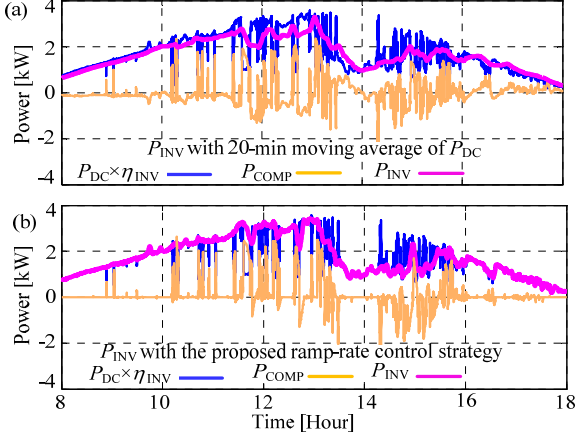

Fig. 11. Mitigation of PV output fluctuation. (a) Using moving average. (b) Using the proposed ramp-rate control strategy.

PV panel DC power, P_{DC} (multiplied by the inverter efficiency), the storage compensation power P_{COMP}, and the inverter output P_{INV} are shown in Fig. 11(a) and 11(b) for the moving average control and the proposed strategy, respectively. For moving average control, a 20-min moving average [9] of P_{DC} is used.

In general, both of the methods (moving average and the proposed approach) can mitigate the fluctuations in PV output, as observed from Fig. 11. However, detailed investigations reveal the specific advantages of the proposed approach. Fig. 12(a) shows P_{DC} and P_{INV} profiles in a shorter window, from 10:00 hour to 13:00 hour. According to the proposed strategy, P_{INV} tracks P_{DC} when the ramp-rate of P_{DC} does not exceed the desired ramp-rate at that time. Therefore, the proposed strategy does not need to operate the storage at all the times. In contrast, (10) suggests that the moving average method needs to continue the storage operation due to the past history of P_{DC}, even if it is not necessary as the ramp-rate is within desired limit. This is observed from P_{COMP} profiles in Fig. 12(b) for the moving average methods and 12(c) for the proposed approach. In Fig. 12(c), zero values of P_{COMP} are highlighted using dotted circular shapes. Examining the P_{COMP} profiles it is found that according to the proposed strategy, the storage device operates for about 50% less time in the 10 hours period (from 8:00 to 18:00 hrs) in comparison to the moving average method. This can contribute to increase the lifetime of a battery storage device.

The percentage ratio of P_{INV} to P_{DC}, based on the profiles in Fig. 12(a), is compared between the proposed approach and moving average method in Fig. 13. Due to the dependency of previous P_{DC} values, P_{INV} obtained from the moving average method is different (lower) than P_{DC}, even during the periods

when P_{DC} exhibits very low fluctuation. In contrast, the proposed approach tracks P_{DC} in those periods and therefore, the P_{INV} to P_{DC} ratio is higher using the proposed approach, as compared to the moving average method.

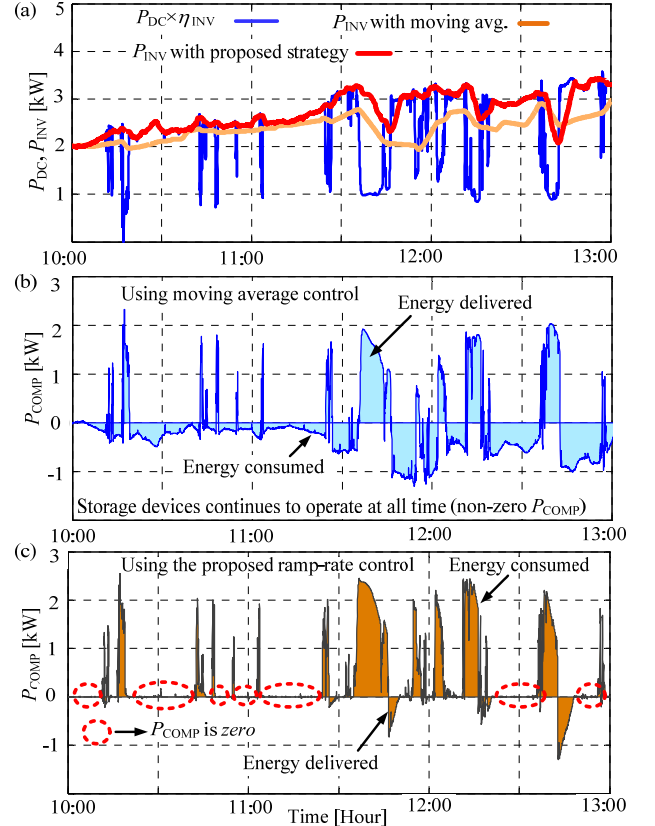Fig. 12. Mitigation of PV output fluctuation. (a) P_{DC} and P_{INV} profiles. (b) P_{COMP} with moving average control. (c) P_{COMP} with the proposed strategy.
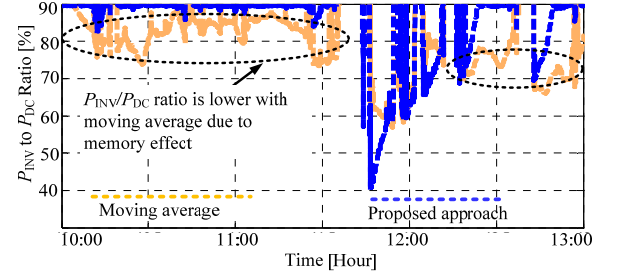

Fig. 13. P_{DC} to P_{INV} ratio.

The ramp-rate profiles of P_{DC} and P_{INV} from 10:00 hour to 13:00 hour are shown in Fig. 14(a); the ramp-rates of P_{INV} can be controlled within a specified limit by operating the storage device according to the proposed strategy. The ramp-rates of P_{INV} with 20-min moving average control of storage device are compared with those obtained using the proposed strategy in Fig. 14(b) for the time period when the maximum negative and positive ramp-rates in P_{DC} appeared. For reference, the ramp-rate of P_{DC} is also included in Fig. 14(b). During the negative fluctuation of P_{DC} with a ramp-rate of -1.767 kW/sec, the proposed strategy controls the P_{INV} ramp-rate at -0.0028 W/sec which comes from the inverse characteristic in (13). With the 20-min moving average, the ramp-rate of P_{INV} is -1.485 W/sec, which is not controlled at this value; rather it is produced as a result of the previous P_{DC} samples over the last

20 min period. During the positive ramping event at 1.725 kW/sec, the ramp-rate with the proposed strategy is 0.0029 W/sec which is controlled using (13), whereas, with the moving average it is 0.0183 W/sec, which is not actually controlled to this value. Although the moving average method provides significant fluctuation mitigation at the expense of operating the storage device all the time, the proposed strategy provides better mitigation during the time of fluctuation with a high ramp-rate (such as the one shown in Fig. 14).
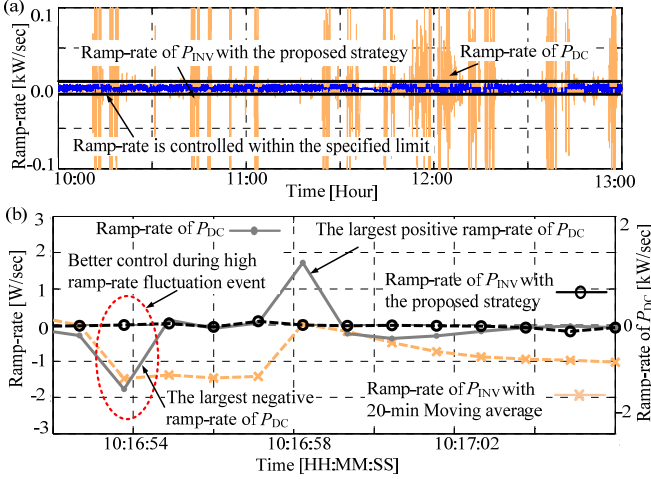

Fig. 14. Ramp-rate control. (a) The ramp-rate profiles of P_{DC} and P_{INV}. (b) Comparison of the P_{INV} ramp-rates obtained using the moving average control and the proposed strategy.

The usefulness of the proposed MARR characteristics in (13) and (14) can also be observed in Fig. 15 where the PV output fluctuation mitigation using the proposed inverse MARR characteristic from 12:00 hours to 13:00 hours is compared with a constant MARR value of 5 W/sec. The proposed inverse MARR and SoC droop based characteristics can mitigate the fluctuation better than a constant MARR value. For reference, the fluctuation mitigation using the 20-min moving average is also included in Fig. 15.
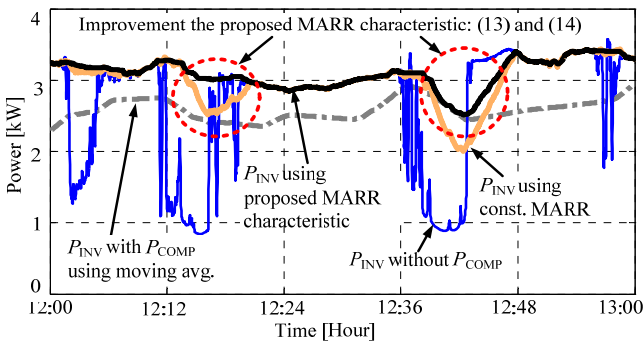

Fig. 15. The usefulness of the proposed inverse characteristic in the improvement of fluctuation mitigation.

The PCC voltage profile at household no. 28 (HH 28) of the test feeder from 10:00 hours to 13:00 hours is shown in Fig. 16(a). For reference, P_{COMP} profile is also shown in Fig. 16(b). When sharp decrease in PCC voltage appears as a result of sudden decrease in PV output, energy storage device is discharged to control the high negative ramp-rates. This action mitigates the associated voltage dips. Again, when sharp rise in PCC voltage appears due to sudden increase in PV output, energy storage device is charged to control the positive ramp-

rates and this action mitigates the sharp voltage rise as well. Without the proposed ramp-rate control strategy, the voltage ramp-rate at 10 hr : 16 min : 54 sec (when the largest negative ramp-rate in the PV output appeared) is -9.3 V/sec and at 10 hr : 16 min : 58 sec (when the largest positive ramp-rate in PV output appeared) is 9.1 V/sec. Controlling the ramp-rate of PV output using the proposed strategy, the PCC voltage ramp-rate is reduced to less than 0.1 mV/sec.
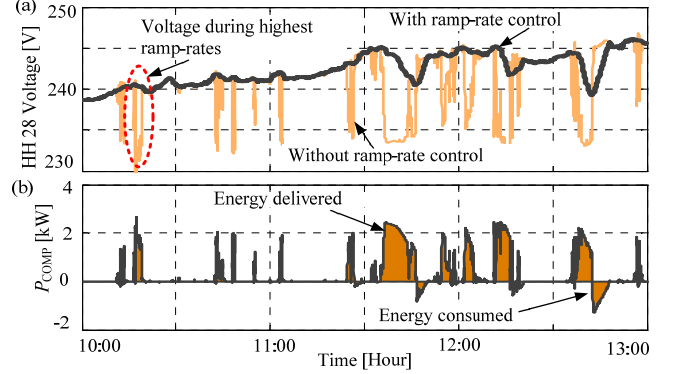

Fig. 16. Mitigation of PCC voltage fluctuation using the proposed strategy. (a) PCC voltage profile. (b) P_{COMP} profile.

The validation of the proposed strategy in a dynamic environment is tested using the proposed PV-storage integrated system model using 1 millisecond time step and the results are presented in Fig. 17. The largest ramp-rate observed in the PV output data used for the daylong simulation is used for this purpose. The dynamic simulation is performed with the data shown in Table II in the Appendix.
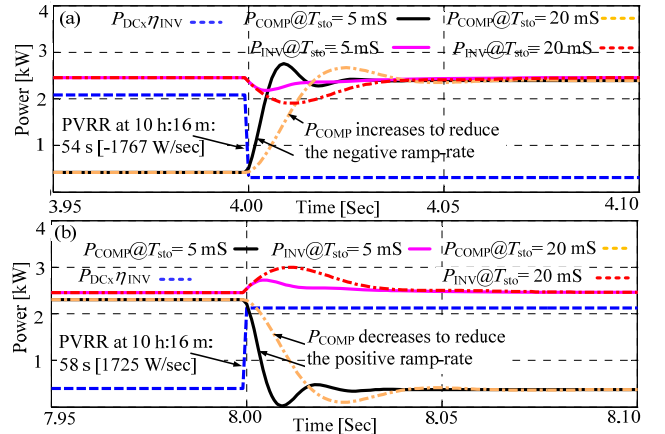

Fig. 17. Performance analysis using the proposed dynamic model. (a) Negative ramp-rate control; (b) Positive ramp-rate control.

The PV output decreases at a ramp-rate of -1.767 kW/sec at 10 hr : 16 min : 54 sec. Fig. 17(a) shows that following the negative ramp-rate of P_{DC}, P_{COMP} increases within a few milliseconds time to increase the P_{INV} at the level that maintains the desired ramp-rate MARR$_\rho$ specified at the time. After 4 seconds time, the P_{DC} again increases with a ramp-rate of 1.725 kW/sec at 10 hr : 16 min : 58 sec. Fig. 17(b) shows that following the positive ramp-rate of P_{DC}, P_{COMP} decreases to the level necessary to maintain the desired ramp-rate of P_{INV} at that time. The impact of the storage time constant T_{sto} is also shown in Fig. 17; P_{INV} with T_{sto} of 5 milliseconds settles down faster and with less swing as compared to the P_{INV} with T_{sto} of 20 milliseconds. Therefore, a storage device

with a fast response time is necessary for a satisfactory mitigation of the fluctuation.

V. EXPERIMENTAL RESULTS

An experimental set-up with a controllable DC power source simulating the PV panel DC power, an Ultratech 12V 7Ah sealed lead-acid battery, a charge/discharge controller (Model: CM3024Z), a PowerBright 400W, 12V DC to 220V AC inverter (Model: ERP400-12), and a Chroma programmable AC/DC electronic load (Model: 63804) is used to verify the main concept of the proposed approach. The experimental set-up is shown in Fig. 18. The waveforms are captured using an Agilent Infiivision (Model: DSO7034A) series oscilloscope.
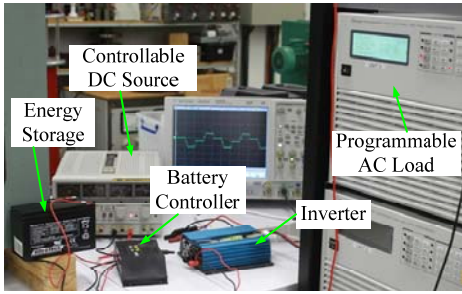

Fig. 18. Experimental set-up for verification of the proposed strategy.

A segment of the real PV generation profile used to obtain the simulation results is used for the experiment where the highest negative and positive ramp-rate of P_{DC} is included. A scale factor is used to scale down the simulation data to comply with the ratings of the equipment. The data points obtained from the simulation are shown in Fig. 19(a) that shows that from the 2nd to the 3rd data point, the PV output decreases at a ramp-rate of -55%/sec of the rated output, then remains at low values of less than 15% of the rated output from the 3rd to 6th data point. Then it increases at a ramp-rate of 53%/sec of the rated output from the 6th to the 7th data point. With the proposed control approach, P_{COMP} is controlled using (13) from the 2nd to the 3rd data points and from the 6th to 7th data points (ramping events). From the 3rd to the 6th data point (post-ramping event), P_{COMP} is controlled using (14). As a result of controlling P_{COMP} according to the proposed strategy, the ramp-rate of P_{INV} is maintained at such a low value over the period of fluctuation (1st to 7th data point) that P_{INV} remains nearly constant, as shown in Fig. 19(a). The captured waveforms of the DC source current, I_{DC}, the battery current, I_{COMP}, and the inverter current I_{INV} at the points (P_1), (P_2), and (P_3) identified in Fig. 19(a), are shown in Fig. 19(b). The time differences among the data points are represented using dashed lines. The decrease of I_{DC} from P_1 to P_2 caused by cloud passing is compensated by the increase of I_{COMP} and therefore, I_{INV} remains nearly constant from P_1 to P_2. The increase of I_{DC} from P_2 to P_3, when the cloud passing is over, makes I_{COMP} to decrease. Therefore, I_{INV} remains nearly constant from P_2 to P_3. The results from this experiment indicate that the proposed strategy would be able to control the

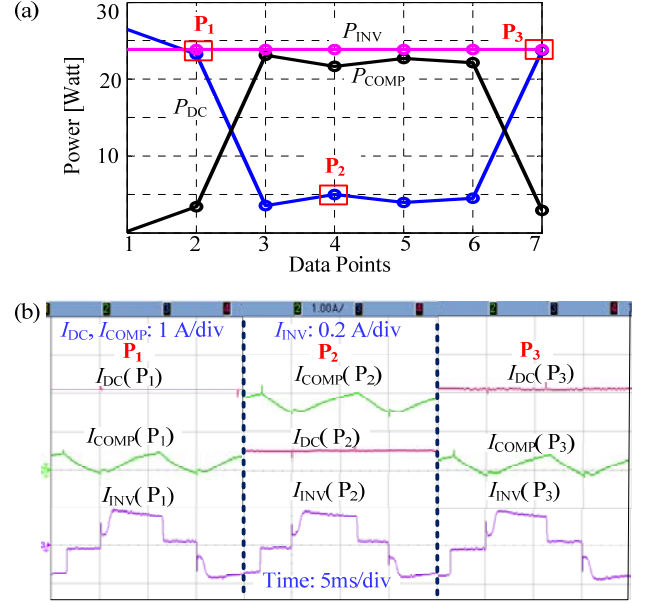ramp-rate of P_{INV} by appropriately controlling the P_{COMP} support.

Fig. 19. Experimental results (a) Data points for experimental verification. (b) Captured current waveforms for points P_1, P_2 and P_3.

VI. CONCLUSION

This paper has proposed a new approach for PV inverter ramp-rate control using an integrated energy storage device. Unlike the traditional moving average method, which is biased by the previous values and does not directly control the ramp-rate at a desired level, the proposed method can limit the ramp-rate within a desired level. An inverse characteristic of the desired ramp-rate with the PV panel output ramp-rate is proposed to improve the fluctuation mitigation performance during the ramping event. Once the ramping event is over, the desired ramp-rate is switched to a droop characteristic with SoC so that the available capacity is taken into account while controlling the ramp-rate. Simulation results show that the mitigation of the PV output fluctuation achieved by the proposed ramp-rate control strategy is comparable to those obtained using the moving average method, while not using the energy storage all the time. Also, during very high ramp-rate events, the proposed strategy can provide tighter control of the ramp-rate due to the inverse characteristic. The mitigation of voltage fluctuation in weak networks caused by PV output fluctuation using the proposed method is also demonstrated. The validity of the proposed strategy has been verified in a dynamic environment using a dynamic model of the PV-storage integrated system developed in this paper. The results from a laboratory experiment using a PV inverter, a battery storage system, and an electronic load demonstrates that the proposed approach is able to control the PV inverter ramp-rate by providing appropriate support from the storage device.

VII. Appendix

TABLE I
SIMULATION PARAMETERS OF THE PROPOSED CONTROL STRATEGY

Parameter	Value
$|RR_{lim}|$, γ	5 W/sec, 0.005
SoC_{ref}, SoC_{LB}, SoC_{UB}, DB_{SoC}	70%, 2.5%, 5%, 2.5%
$MARR_{min}$, $MARR_{max}$, DB_{MARR}	$MARR\rho$, 5 W/sec, (5-$MARR_{min}$)
SoC_{max}, DoD_{max}	100%, 40%

TABLE II
PARAMETERS USED FOR DYNAMIC SIMULATION

Parameter	Value
T_{inv}, T_{sto}, T_{meas}	20 mS, 5 mS, 3 mS
K_P, K_I	2.30, 470

VIII. References

[1] W. Jewell and R. Ramakumar, "The Effects of Moving Clouds on Electric Utilities with Dispersed Photovoltaic Generation," *IEEE Transactions on Energy Conversion,* vol. EC-2, pp. 570-576, 1987.

[2] E. C. Kern, E. M. Gulachenski, and G. A. Kern, "Cloud effects on distributed photovoltaic generation: slow transients at the Gardner, Massachusetts photovoltaic experiment," *IEEE Transactions on Energy Conversion,* vol. 4, pp. 184-190, 1989.

[3] C. Trueblood, S. Coley, T. Key, L. Rogers, A. Ellis, C. Hansen, and E. Philpot, "PV Measures Up for Fleet Duty : Data from a Tennessee Plant Are Used to Illustrate Metrics That Characterize Plant Performance," *IEEE Power and Energy Magazine,* vol. 11, pp. 33-44, 2013.

[4] J. Johnson, B. Schenkman, A. Ellis, J. Quiroz, and C. Lenox.Sandia National Laboratories. *Initial Operating Experience of the La Ola 1.2-MW Photovoltaic System* [Online]. Available: http://energy.sandia.gov/wp/wp-content/gallery/uploads/SAND2011-8848_Lanai_DOE_Report_FINAL.pdf

[5] NREL. *1-Second Global Horizontal Irradiance Oahu, Hawaii* [Online]. Available: http://www.nrel.gov/midc/oahu_archive/

[6] S. Abdollahy, A. Mammoli, F. Cheng, A. Ellis, and J. Johnson, "Distributed compensation of a large intermittent energy resource in a distribution feeder," in *IEEE PES Innovative Smart Grid Technologies*, Washington, DC, USA, 24-27 Feb. 2013, pp. 1-6.

[7] S. Sayeef, S. Heslop, D. Cornforth, T. Moore, S. Percy, J. K. Ward, A. Berry, and D. Rowe.CSIRO. (June 2012). *Solar intermittency: Australia's clean energy challenge. Characterising the effect of high penetration solar intermittency on Australian electricity networks.* [Online]. Available: https://publications.csiro.au/rpr/download?pid=csiro:EP121914&dsid=DS1

[8] H. Sugihara, K. Yokoyama, O. Saeki, K. Tsuji, and T. Funaki, "Economic and Efficient Voltage Management Using Customer-Owned Energy Storage Systems in a Distribution Network With High Penetration of Photovoltaic Systems," *IEEE Transactions on Power Systems,* vol. 28, pp. 102-111, 2013.

[9] N. Kakimoto, H. Satoh, S. Takayama, and K. Nakamura, "Ramp-Rate Control of Photovoltaic Generator With Electric Double-Layer Capacitor," *IEEE Transactions on Energy Conversion* vol. 24, pp. 465-473, 2009.

[10] T. Kinjo, T. Senjyu, N. Urasaki, and H. Fujita, "Output levelling of renewable energy by electric double-layer capacitor applied for energy storage system," *IEEE Transactions on Energy Conversion,* vol. 21, pp. 221-227, 2006.

[11] T. Monai, I. Takano, H. Nishikawa, and Y. Sawada, "A collaborative operation method between new energy-type dispersed power supply and EDLC," *IEEE Transactions on Energy Conversion,* vol. 19, pp. 590-598, 2004.

[12] K. S. Tam, P. Kumar, and M. Foreman, "Enhancing the utilization of photovoltaic power generation by superconductive magnetic energy storage," *IEEE Transactions on Energy Conversion,* vol. 4, pp. 314-321, 1989.

[13] S. Rahman and K. S. Tam, "A feasibility study of photovoltaic-fuel cell hybrid energy system," *IEEE Transactions on Energy Conversion,* vol. 3, pp. 50-55, 1988.

[14] T. D. Hund, S. Gonzalez, and K. Barrett, "Grid-Tied PV system energy smoothing," in *Photovoltaic Specialists Conference (PVSC)*, Honolulu, HI, USA, 20-25 Jun., 2010, pp. 2762-2766.

[15] J. Traube, L. Fenglong, D. Maksimovic, J. Mossoba, M. Kromer, P. Faill, S. Katz, B. Borowy, S. Nichols, and L. Casey, "Mitigation of Solar Irradiance Intermittency in Photovoltaic Power Systems With Integrated Electric-Vehicle Charging Functionality," *IEEE Transactions on Power Electronics,* vol. 28, pp. 3058-3067, 2013.

[16] S. G. Tesfahunegn, Ø. Ulleberg, P. J. Vie, and T. M. Undeland, "PV Fluctuation Balancing Using Hydrogen Storage–a Smoothing Method for Integration of PV Generation into the Utility Grid," *Energy Procedia,* vol. 12, pp. 1015-1022, 2011.

[17] L. Xiangjun, H. Dong, and L. Xiaokang, "Battery Energy Storage Station (BESS)-Based Smoothing Control of Photovoltaic (PV) and Wind Power Generation Fluctuations," *IEEE Transactions on Sustainable Energy,* vol. 4, pp. 464-473, 2013.

[18] C. J. Coe, A. N. Hurst, M. I. Hardin, M. C. Such, and R. T. Jennings.(Nov. 2011, US Patent 20110273129). *Managing Renewable Power Generation* [Online]. Available: https://docs.google.com/viewer?url=www.google.com/patents/US20110273129.pdf

[19] C. A. Hill, M. C. Such, C. Dongmei, J. Gonzalez, and W. M. Grady, "Battery Energy Storage for Enabling Integration of Distributed Solar Power Generation," *IEEE Transactions on Smart Grid,* vol. 3, pp. 850-857, 2012.

[20] A. Ellis, D. Schoenwald, J. Hawkins, S. Willard, and B. Arellano, "PV output smoothing with energy storage," in *Photovoltaic Specialists Conference (PVSC)*, Austin, TX, USA., 3-8 Jun., 2012, pp. 1523-1528.

[21] M. J. E. Alam, K. M. Muttaqi, and D. Sutanto, "Mitigation of Rooftop Solar PV Impacts and Evening Peak Support by Managing Available Capacity of Distributed Energy Storage Systems," *Accepted for a future issue of IEEE Transactions on Power Systems.*

[22] H. Chen, T. N. Cong, W. Yang, C. Tan, Y. Li, and Y. Ding, "Progress in electrical energy storage system: A critical review," *Progress in Natural Science,* vol. 19, pp. 291-312, 2009.

[23] B. Espinar and D. Mayer.International Energy Agency. July 2011. *The role of energy storage for mini-grid stabilization* [Online]. Available: http://www.iea-pvps-task11.org/HTMLobj-187/Act_24_Final.pdf

[24] Mathworks. (Oct. 2013). *PID tuning algorithm for linear plant model* [Online]. Available: http://www.mathworks.com.au/help/control/ref/pidtune.html

Biographies

M J E Alam (S'10) obtained his B Sc and M Sc degree in EEE from Bangladesh University Engineering and Technology in 2005 and 2009, respectively. At present, he is working towards PhD degree at the University of Wollongong, New South Wales, Australia. His research interest includes modeling and analysis of power systems considering the impacts of distributed and renewable energy resources. He has worked in the electric utility industry in Bangladesh for 4.5 years

K M Muttaqi (M'01, SM'05) received the Ph.D. degree from Multimedia University, Malaysia, in 2001. Currently, he is an Associate Professor at the School of Electrical, Computer, and Telecommunications Engineering, University of Wollongong, Wollongong, Australia. He is an Associate Editor of IEEE Transactions on Industry Applications. His special fields of interests include distributed generation, renewable energy, power system planning, intelligent grid, and power system reliability.

D Sutanto (SM'89) obtained his BEng. (Hons) and PhD from the University of Western Australia. He is presently the Professor of Power Engineering at the University of Wollongong, Australia. His research interests include power system planning, analysis and harmonics, FACTS and Battery Energy Storage systems. He is a Senior Member of IEEE. He is currently the IEEE IAS Area Chair for Region 10 (Asia Pacific).